Multipole analysis of radio-frequency reactions in ultracold atoms

Betzalel Bazak, Evgeny Liverts, and Nir Barnea
The Racah Institute of Physics, The Hebrew University, 91904 Jerusalem, Israel
(Received 9 May 2012; published 10 October 2012)

Using the multipole expansion, we analyze photoinduced reactions in an ultracold atomic gas composed of identical neutral bosons. While the Franck-Condon factor dominates the photoinduced spin-flip reactions, we have found that for a frozen-spin process in which the atomic spins are conserved, the reaction rate is governed by the monopole r^2 and the quadrupole terms. Consequently, the dependence of the frozen-spin reaction rate on the photon wave number k acquires an extra k^4 factor in comparison to the spin-flip process. Comparing the relative strength of the r^2 and quadrupole modes in dimer photoassociation, we predict that the mutual importance of these two modes changes with temperature and scattering length.

DOI: 10.1103/PhysRevA.86.043611 PACS number(s): 67.85.−d, 25.20.−x, 25.10.+s, 31.15.ac

I. INTRODUCTION

Radio-frequency (rf) association of molecules in ultracold atomic traps is an invaluable experimental tool for studying the universal properties of few-body systems [1,2]. In such experiments [3–10], rf induced dimer or trimer formation leads to an enhanced atom loss rate due to a larger probability for three-body recombination. The measured atom loss rate as a function of the rf field frequency incorporates the data about the various molecular thresholds and structures, and can be used to calibrate the two-body scattering length and to measure the three-body binding energy.

Photointegration of molecules, where resonant rf radiation is used to stimulate photon emission, is closely related, through time reversal, to electroweak reactions in light nuclei. In fact, rf photoreactions inducing an atomic spin-flip are governed by the Franck-Condon factor. This factor is the atomic analog of the Fermi operator, which at low momentum transfer describes the charged vector-current neutrino induced isospin-flip reactions in nuclear systems. The nuclear analog to frozen-spin rf reactions is photoabsorption, where an incoming photon dissociates the nucleus. For example, photoreactions within the α-cluster model of nuclei such as ^{12}C and ^{16}O are governed by the same physical mechanisms studied here. Therefore, studying rf photoreactions in ultracold atomic systems can be instrumental for understanding the nuclear dynamics, the complicated nuclear continuum, and for predicting unmeasurable electroweak cross sections of astrophysical importance.

Previous analyses of these rf experiments [11–14] have relied on the Franck-Condon factor estimating the transition rates. While this approach is appropriate for describing spin-flip reactions, it is not suitable for frozen-spin reactions. In Ref. [15], we have studied the quadrupole contribution to the frozen-spin response of a bound bosonic trimer. In this article, we present a complete multipole analysis of the rf association process forming a bound molecule composed of N identical bosons. We show that the spin-flip and frozen-spin processes differ by their operator structure and by the deexcitation modes that contribute to the photoassociation rate. We apply our results to study frozen-spin dimer formation. We focus on bosonic alkali-metal atoms, in which a single s-shell valence electron is coupled to a half-integer spin nucleus to form a boson. This is the case for ^{7}Li, ^{23}Na, ^{39}K, ^{41}K, ^{85}Rb, ^{87}Rb, and ^{133}Cs. Extension of our results to other atoms and fermionic isotopes is rather simple but is beyond the scope of the current manuscript.

II. THEORETICAL FRAMEWORK

In ultracold atomic traps, the trapped particles are subject to an external magnetic field $\boldsymbol{B} = B\hat{z}$ applied to control the interatomic interaction, i.e. the scattering length, through a Feshbach resonance. Consequently, the energy of the system is dominated by the interactions of the valence electron spin $S = \frac{1}{2}$ with the external and the nuclear magnetic fields. The Zeeman interaction with the external magnetic field reads $-g\mu_B \boldsymbol{S}\cdot\boldsymbol{B}$, where g is the electron g factor and μ_B is the Bohr magneton [16]. The hyperfine spin-nucleus contact interaction $\hbar\omega_{\rm hf}\boldsymbol{I}\cdot\boldsymbol{S}$ couples the electron with the nuclear spin $\boldsymbol{I}$, where $\omega_{\rm hf}$ is the hyperfine splitting frequency. When both interactions are comparable, the total spin $\boldsymbol{F} = \boldsymbol{I} + \boldsymbol{S}$ is not a good quantum number, however its projection m_F is.

To be specific, we consider $I = \frac{3}{2}$, the case for ^{7}Li, ^{23}Na, ^{39}K, ^{41}K, and ^{87}Rb. The atomic spin state composition in the $|m_S, m_I\rangle$ basis,

$$|m_F\rangle = \sin\theta_{m_F}\left|1/2, m_F - 1/2\right\rangle + \cos\theta_{m_F}\left|1/2, m_F + 1/2\right\rangle,$$

is given by

$$\tan\theta_{m_F} = \begin{cases} \infty, & m_F = 2, \\ (1 - 2\eta - 2\sqrt{1-\eta+\eta^2})/\sqrt{3}, & m_F = 1, \\ -\eta - \sqrt{1+\eta^2}, & m_F = 0, \\ -(1 + 2\eta + 2\sqrt{1+\eta+\eta^2})/\sqrt{3}, & m_F = -1, \end{cases} \tag{1}$$

for the low-energy branch states. Here $\eta = g\mu_B B/2\hbar\omega_{\rm hf}$ is the ratio between the Zeeman and the hyperfine splitting.

In photoassociation experiments, an rf radiation of a few MHz is applied to the ultracold atomic gas. When the photon energy matches, stimulated emission occurs and a molecule is formed. Fermi's Golden Rule dictates the transition rate of such a process to be

$$r_{i\to f} = \frac{2\pi}{\hbar}\bar{\sum_i}\sum_f |\langle f, \boldsymbol{k}\rho|\hat{H}_I|i\rangle|^2\delta(E_i - E_f - \hbar\omega_k), \tag{2}$$

where $\bar{\sum}_i$ averages on the appropriate initial states and $\sum_f$ sums on the final states. Specifically, $|i\rangle$ is the continuum state,

$\boldsymbol{k}\rho$ is the emitted photon momentum and polarization, and $|f\rangle$ is the formed N-body bound state.

The interaction Hamiltonian $\hat{H}_I = -\frac{e}{c}\int d\boldsymbol{x}\, \boldsymbol{J}(\boldsymbol{x})\cdot\boldsymbol{A}(\boldsymbol{x})$ between an atomic system and an electromagnetic (EM) radiation field $\boldsymbol{A}$ is defined by the current operator $\boldsymbol{J}$ composed of convection and magnetization terms, $\boldsymbol{J}(\boldsymbol{x}) = \boldsymbol{J}_c(\boldsymbol{x}) + c\nabla\times\boldsymbol{\mu}(\boldsymbol{x})$. For a system of neutral atoms interacting with long-wavelength radiation, $\boldsymbol{J}_c \approx 0$, and the interaction between the radiation field and the system occurs through the magnetization density $e\boldsymbol{\mu}(\boldsymbol{x}) = g\mu_B\sum_i \boldsymbol{S}_i\delta(\boldsymbol{x}-\boldsymbol{r}_i)$. Using box normalization of volume Ω, the EM field reads $\boldsymbol{A}(\boldsymbol{x}) = \sum_{k,\rho}\sqrt{\frac{\hbar c^2}{2\Omega\omega_k}}\hat{\boldsymbol{e}}_{\boldsymbol{k}\rho}(a^\dagger_{\boldsymbol{k}\rho}e^{i\boldsymbol{k}\cdot\boldsymbol{x}} + \text{H.c.})$, where $\rho = 1,2$ are the photon linear polarizations, ω_k is its frequency and $\boldsymbol{k}$ is its momentum.

For an atomic system, we can assume that the initial and final matter wave functions can be written as a product of spin and configuration space terms, $\Psi = \Phi_{LM_L}\chi_{M_F}$, where $\Phi_{LM_L} = \Phi_{LM_L}(\boldsymbol{r}_1,\boldsymbol{r}_2,\ldots,\boldsymbol{r}_A)$ is a symmetric N-particle wave function with angular momentum quantum numbers LM_L, and $\chi_{M_F} = \mathcal{S}\,[|m_F(1)\rangle|m_F(2)\rangle\cdots|m_F(A)\rangle]$ is the symmetrized spin wave function with magnetic quantum number $M_F = \sum_j m_F(j)$. Using this factorization, the transition matrix element in Eq. (2) takes the form

$$\langle f,\boldsymbol{k}\rho|\hat{H}_I|i\rangle = -ig\mu_B\sqrt{\frac{\hbar c^2}{2\Omega\omega_k}}\sum_{j=1}^{N} \left\langle\chi^f_{M'_F}\middle|\boldsymbol{S}_j\cdot(\boldsymbol{k}\times\hat{\boldsymbol{e}}_{\boldsymbol{k}\rho})\middle|\chi^i_{M_F}\right\rangle\left\langle\Phi^f_{L'M'_L}\middle|e^{i\boldsymbol{k}\cdot\boldsymbol{r}_j}\middle|\Phi^i_{LM_L}\right\rangle. \tag{3}$$

The spin operator can be written in spherical notation, $\boldsymbol{S}\cdot(\boldsymbol{k}\times\hat{\boldsymbol{e}}_{\boldsymbol{k}\rho}) = \sum_\lambda(-)^\lambda S_{-\lambda}\cdot(\boldsymbol{k}\times\hat{\boldsymbol{e}}_{\boldsymbol{k}\rho})_\lambda$, where $\lambda = 0,\pm1$. To calculate this quantity, the laboratory $\hat{z}$ axis is defined by the static magnetic field. The rotation from the laboratory reference frame, $(\hat{x},\hat{y},\hat{z})$, to the photon reference frame, $(\hat{e},\hat{k}\times\hat{e},\hat{k})$, is represented by Euler angles (α,β,γ). Then, $(\hat{k}\times\hat{e})\cdot\hat{z} = -\sin\gamma\sin\beta$, and $|(\hat{k}\times\hat{e})_{\pm1}|^2 = (1-\sin^2\gamma\sin^2\beta)/2$.

For rf radiation, the photon wavelength is much larger than the typical dimension of the system R, therefore $kR \ll 1$ and the lowest order in kR dominates the interaction. The first contribution depends on the photon energy versus the energy difference between adjacent Zeeman states.

Using Eq. (1), the spin matrix elements can be easily calculated to give

$$\langle m'_F|S_\lambda|m_F\rangle = \delta_{m_F+\lambda,m'_F}\begin{cases}\sin\theta_{m'_F}\cos\theta_{m_F}, & \lambda=+1,\\ -\frac{1}{2}\cos2\theta_{m_F}, & \lambda=0,\\ \sin\theta_{m_F}\cos\theta_{m'_F}, & \lambda=-1.\end{cases} \tag{4}$$

If the photon can induce a Zeeman state change, i.e., spin-flip, the leading contribution comes at order k. Energy is delivered to the system through the spin matrix element, and we can approximate $e^{ix}\simeq 1$ to get

$$|\langle f,\boldsymbol{k}\rho|\hat{H}_I|i\rangle|^2 = \frac{g^2\mu_B^2\hbar ck(1-\sin^2\gamma\sin^2\beta)N^2}{4\Omega} \times\sum_{\lambda=\pm1}\left|\left\langle\chi^f_{M'_F}\middle|S_{j,\lambda}\middle|\chi^i_{M_F}\right\rangle\right|^2 \times\left|\left\langle\Phi^f_{L'M'_L}\middle|\Phi^i_{LM_L}\right\rangle\right|^2\delta_{L,L'}\delta_{M_L,M'_L}. \tag{5}$$

The factor N^2 results from utilizing the symmetry of the wave function and $S_{j,\lambda}$ is the magnetic moment operator of any specific particle j. The last term on the right-hand side (rhs) of Eq. (5) is just the Franck-Condon factor.

In frozen spin reactions, $\lambda = 0$, and the rf photon does not affect the spin structure of the system. Therefore, $M'_F = M_F$, $|\chi^f_{M_F}\rangle = |\chi^i_{M_F}\rangle$, and the transition matrix element can be written as

$$\langle f,\boldsymbol{k}\rho|\hat{H}_I|i\rangle = -ig\mu_B\sqrt{\frac{\hbar c^2}{2\Omega\omega_k}}k\sin\gamma\sin\beta\langle S_0\rangle \times\left\langle\Phi^f_{L'M'_L}\middle|\sum_{j=1}^{N}e^{i\boldsymbol{k}\cdot\boldsymbol{r}_j}\middle|\Phi^i_{LM_L}\right\rangle, \tag{6}$$

where $\langle S_0\rangle = \langle\chi^i_{M_F}|S_{1,0}|\chi^i_{M_F}\rangle$ is the average single-particle magnetic moment.

In the long-wavelength limit, the leading contributions to the photoreaction process are

$$\sum_{j=1}^{N}e^{i\boldsymbol{k}\cdot\boldsymbol{r}_j} \approx N + i\sum_{j=1}^{N}\boldsymbol{k}\cdot\boldsymbol{r}_j - \sum_{j=1}^{N}\frac{k^2r_j^2}{6} - \sum_{j=1}^{N}4\pi\frac{k^2r_j^2}{15}\sum_m Y_{2-m}(\hat{k})Y_{2m}(\hat{r}_j), \tag{7}$$

where Y_{lm} are the spherical harmonics. The difference between the four operators in Eq. (7) is clear. The first operator is proportional to 1 and stands for elastic interaction. For photon emission, this kind of interaction defies energy conservation. The second term is just the dipole operator, which for identical particles is proportional to the center of mass and hence does not affect the relative motion of the atoms. Therefore, the only contributions to such excitation arises from the r^2 and the quadrupole terms. Consequently, the transition probability scales as k^5. Summing over the initial and final magnetic numbers M_L and M'_L, the transition matrix element reads

$$\sum_{M_L}\sum_{M'_L}|\langle f,\boldsymbol{k}\rho|\hat{H}_I|i\rangle|^2 = \frac{4\pi\hbar ck^5g^2\mu_B^2\sin^2\gamma\sin^2\beta N^2}{2\Omega}|\langle S_0\rangle|^2 \times\left(\frac{1}{6^2}\left|\left\langle\Phi^f_{L'}\middle\|r_j^2Y_0\middle\|\Phi^i_L\right\rangle\right|^2 + \frac{1}{15^2}\left|\left\langle\Phi^f_{L'}\middle\|r_j^2Y_2(\hat{r}_j)\middle\|\Phi^i_L\right\rangle\right|^2\right). \tag{8}$$

Here, like in Eq. (5), we have used the symmetry of the wave function, and $\boldsymbol{r}_j$ is the coordinate of any of the particles, $j = 1,\ldots N$. Comparing Eqs. (5) and (8), the difference between spin-flip and frozen-spin reactions is evident. To begin with, the frozen spin acquires an extra k^4 factor suppressing the reaction rate. Then we see that, whereas the leading configuration space spin-flip operator is proportional to the unit operator, like the Fermi operator in nuclear physics, for frozen-spin reactions we identify two competing modes of order k^2: one is the r^2 operator and the other is just the quadrupole operator.

III. DIMER PHOTOASSOCIATION

Once the operator structure of the transition rate is established, we will focus our attention on frozen-spin photoassociation reactions trying to estimate the relative importance of the two reaction modes. To this end, we consider the case of dimer formation, which under certain simplifying assumptions can be calculated analytically.

In the universal regime, where the scattering length is much larger than the potential range, one can approximate the wave functions by their asymptotic behavior. The dimer bound state with binding energy E_B is an s-wave state, and $\Phi^f_{00}(\boldsymbol{r}) = Y_{00}\,\varphi_B(r)/r$, where $\boldsymbol{r} = \boldsymbol{r}_2 - \boldsymbol{r}_1$ is the relative coordinate, $\varphi_B(r) \cong \sqrt{2\kappa}e^{-\kappa r}$ and $\kappa = \sqrt{m|E_B|/\hbar^2}$. For the initial (continuum) states, the asymptotic scattering solution is used, i.e., $\Phi^i_{LM}(\boldsymbol{r}) = Y_{LM}\,\phi_L(r)/r$, where $\phi_L(r) = \sqrt{2/R}qr[j_L(qr)\cos\delta_L - y_L(qr)\sin\delta_L]$, δ_L is the phase shift, j_L and y_L are the spherical Bessel functions of the first and second kind, q is the relative momentum, and the wave function is normalized in a sphere of radius R.

Given the $L' = 0$ dimer ground state, the r^2 term corresponds to $L = 0$ s-wave formation, while the quadrupole term corresponds to $L = 2$ d-wave formation. Using $|\langle 0\|Y_0\|0\rangle|^2 = 1/4\pi$ and $|\langle 2\|Y_2\|0\rangle|^2 = 5/4\pi$,

$$\left|\left\langle\Phi^f_0\middle\|r^2Y_0\middle\|\Phi^i_0\right\rangle\right|^2 = \frac{1}{4\pi}I_s^2, \quad \left|\left\langle\Phi^f_0\middle\|r^2Y_2\middle\|\Phi^i_2\right\rangle\right|^2 = \frac{5}{4\pi}I_d^2. \tag{9}$$

Here $I_s = \int_0^\infty \varphi^*_B(r)\phi_0(r)r^2dr$, and the same for I_d replacing ϕ_0 by ϕ_2. The transformation to the relative coordinate r in Eq. (9) adds an extra factor of $1/16$ in Eq. (8).

For the s-wave mode, the radial integration yields

$$I_s = \frac{4q}{(q^2+\kappa^2)^3}\sqrt{\frac{\kappa}{R}}\left[(3\kappa^2 - q^2)\cos\delta_0 - \frac{\kappa}{q}(3q^2-\kappa^2)\sin\delta_0\right]. \tag{10}$$

At low scattering energy, the s-wave phase shift takes the form $q\cot\delta_0 \cong -\frac{1}{a_s} + r_{\rm eff}q^2/2$, where a_s is the scattering length and $r_{\rm eff}$ is the effective range. The dimer's binding energy is connected to these parameters by the relation [17] $\kappa = \frac{1}{a_s} + r_{\rm eff}\kappa^2/2$.

For the d-wave mode, the radial integration yields

$$I_d = \frac{2q}{(q^2+\kappa^2)^3}\sqrt{\frac{\kappa}{R}}\left[8q^2\cos\delta_2 + \frac{\kappa}{q^3}(15q^4 + 10q^2\kappa^2 + 3\kappa^4)\sin\delta_2\right]. \tag{11}$$

For short-range potentials, $\delta_L \approx q^{2L+1}$ as $q \longrightarrow 0$, thus $\delta_2 \approx (a_d q)^5$, where a_d is the d-wave "scattering length." We note that for the van der Waals potential, the correct threshold behavior is $\delta_2 \approx \pm(a_d q)^4$ [18]. As long as a_d is of the order of the effective range, it is safe to assume $\delta_2 \approx 0$.

The relative contribution of the s,d modes to the dimer formation is displayed in Fig. 1, where the last term in parentheses on the rhs of Eq. (8) is presented normalized, along with the s and d components. From the figure, it can be seen that the s-wave association is peaked around $q = \kappa/2$, while

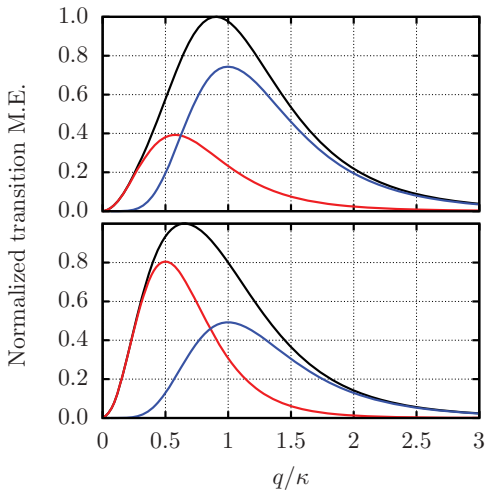

FIG. 1. (Color online) The normalized two-body transition matrix element, Eq. (8), as a function of the relative momentum q/κ. The sum (black), r^2 (red, peaked at $q = \kappa/2$), and quadrupole (blue, peaked at $q = \kappa$) terms are given for $a/r_{\rm eff} = 2$ (upper panel) and $a/r_{\rm eff} = 200$ (lower panel).

the d-wave association is peaked at $q = \kappa$. For a small $a_s/r_{\rm eff}$ ratio, the d-wave is the dominant mode, but as we approach the unitary limit $a_s/r_{\rm eff} \longrightarrow \infty$ the s-wave becomes dominant. We note, however, that as the $a_s/r_{\rm eff}$ ratio become smaller, finite range corrections, ignored here, become more important. In photoassociation experiments, angular analysis is impossible and therefore the different energy dependence of the two dimer formation modes, Fig. 1, can be used to distinguish between them. As it stands, the large overlap between the two modes will certainly complicate such an attempt.

The average of the initial states $\bar{\sum}_i$ and the sum over the final states $\sum_f$ are the last components needed for evaluating the dimer association rate, Eq. (2). The initial two-body state $|i\rangle = |qLM_L\rangle$ describes two atoms in the continuum with relative momentum q and angular momentum L, M_L. The average on these states takes the form

$$\bar{\sum_i} = \sum_{L=0}^{\infty}\sum_{M_L=-L}^{L}\int_0^\infty dq\,P(qLM_L), \tag{12}$$

where $P(qLM_L)$ is the probability of finding an atomic pair in an internal state $|qLM_L\rangle$ due to thermal distribution. We assume that the system is in thermal equilibrium with temperature $T > T_{\rm BEC}$ higher than the condensation temperature. The partition function of a pair confined in a sphere of radius R is given by [19]

$$\mathcal{Z} = \sum_{n\in\text{bound states}} e^{-\beta E_n} + \frac{1}{\pi}\int_0^\infty dq\sum_{L=0}^{L_{\rm max}}(2L+1)\left(R + \frac{d\delta_L}{dq}\right)e^{-\beta\hbar^2q^2/m}. \tag{13}$$

Given q, finite R imposes a cutoff $L_{\rm max} \approx qR$ on L. For $L = 0,2$ and large enough R, we can safely assume that $P(qLM_L) = P(q) = \frac{1}{\mathcal{Z}}\frac{R}{\pi}e^{-\beta\hbar^2q^2/m}$.

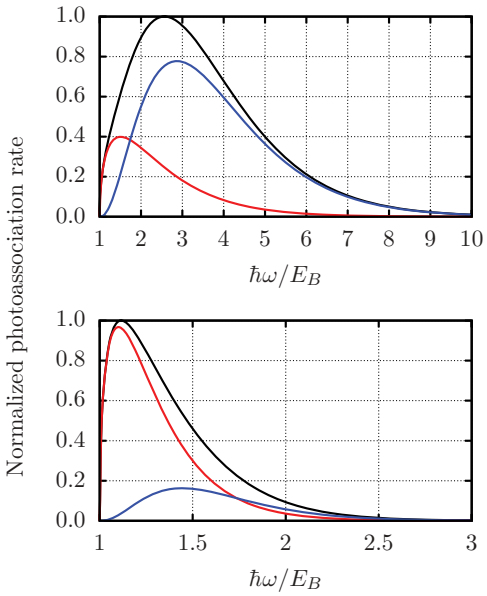

FIG. 2. (Color online) Normalized dimer photoassociation rate as a function of rf photon frequency. The total (black), r^2 (red, low-energy peak), and quadrupole (blue) rates are presented for ^{7}Li with $a_s = 1000a_0$ at $T = 5$ μK (lower panel) and at $T = 25$ μK (upper panel).

The sum $\sum_f$ contains all possible dimer quantum numbers and all possible photons weighted by the emission function,

$$\sum_f = \frac{\Omega}{(2\pi)^3} \sum_{\rho, L', M_L'} \int d\boldsymbol{k}(1 + N_{\boldsymbol{k}\rho}), \tag{14}$$

where $N_{\boldsymbol{k}\rho}$ is the number of photons with momentum $\boldsymbol{k}$ and polarization ρ in the initial state. The stimulating rf radiation is a narrow distribution centered at some $\boldsymbol{k}_{\rm rf}$. Therefore, $N_{\boldsymbol{k}\rho} \approx N_{\boldsymbol{k}_{\rm rf}\rho_{\rm rf}}\delta(\boldsymbol{k} - \boldsymbol{k}_{\rm rf})\delta_{\rho,\rho_{\rm rf}}/\Omega$, where $\boldsymbol{k}_{\rm rf}$ is the momentum of the stimulating rf field and $\rho_{\rm rf}$ is its polarization.

Substituting Eqs. (8), (12), and (14) into Fermi's Golden Rule (2), the dimer formation rate is given by

$$r_{i\to f} = \frac{g^2\mu_B^2 c k_{\rm rf}^5 m}{16(2\pi)^2\hbar^2 q} \frac{N_{\boldsymbol{k}_{\rm rf},\rho_{\rm rf}}}{\Omega} P(q) \times |\langle S_0\rangle|^2 \sin^2\gamma \sin^2\beta \left(\frac{1}{6^2} I_s^2 + \frac{5}{15^2} I_d^2\right). \tag{15}$$

The relative momentum q is connected to the photon wave number through energy conservation, $\hbar^2 q^2/m = E_B + \hbar c k_{\rm rf}$.

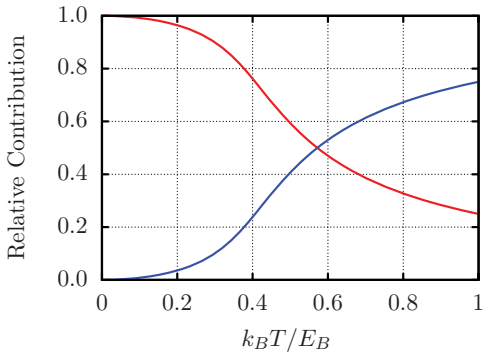

FIG. 3. (Color online) The relative contribution of the s [red (light gray)] and d modes to the resonance peak as a function of temperature k_BT/E_B.

The relative importance of s,d modes shifts with temperature. This point is demonstrated in Figs. 2 and 3. In Fig. 2, we present the s,d rates to the photoassociation of ^{7}Li dimers at $a = 1000a_0$, where a_0 is the Bohr radius, for $T = 5$ and 25 μK. The relative contribution of the r^2 and the quadrupole to the resonance peak is displayed in Fig. 3. It is evident that at low temperatures, the s mode is dominant. The importance of the d mode grows with the ratio k_BT/E_B. Therefore, we can conclude that for small k_BT/E_B values, the photoassociation is an s-wave process, while for large values it is a d-wave process.

IV. CONCLUSIONS

Summing up, in this work we have studied the photoresponse of ultracold atomic gases. Comparing spin-flip and frozen-spin experiments, we have found that the reaction mechanism is quite different in these two processes. While the spin-flip reaction is dominated by the well-known Franck-Condon factor, for the frozen-spin process the reaction rate is governed by the two competing r^2 and quadrupole modes. Comparing the relative strength of these modes in dimer photoassociation, we predict that the mutual importance of these two modes changes with temperature and scattering length. The implications of these results on photoassociation experiments and on trimer formation rates have yet to be studied.

ACKNOWLEDGMENTS

This work was supported by the Israel Science Foundation (Grant No. 954/09). The authors would like to thank L. Khaykovich, S. Jochim, and N. Nevo Dinur for their useful comments and suggestions during the preparation of this work.

[1] C. H. Greene, Phys. Today **63**(3), 40 (2010).
[2] E. Braaten and H.-W. Hammer, Phys. Rep. **428**, 259 (2006).
[3] S. T. Thompson, E. Hodby, and C. E. Wieman, Phys. Rev. Lett. **95**, 190404 (2005).
[4] S. B. Papp and C. E. Wieman, Phys. Rev. Lett. **97**, 180404 (2006).
[5] C. Weber, G. Barontini, J. Catani, G. Thalhammer, M. Inguscio, and F. Minardi, Phys. Rev. A **78**, 061601(R) (2008).
[6] T. Lompe *et al.*, Science **330**, 940 (2010).
[7] N. Gross, Z. Shotan, S. Kokkelmans, and L. Khaykovich, Phys. Rev. Lett. **105**, 103203 (2010).
[8] N. Gross, Z. Shotan, O. Machtey, S. Kokkelmans, and L. Khaykovich, C. R. Phys. **12**, 4 (2011).
[9] S. Nakajima, M. Horikoshi, T. Mukaiyama, P. Naidon, and M. Ueda, Phys. Rev. Lett. **106**, 143201 (2011).

[10] O. Machtey, Z. Shotan, N. Gross, and L. Khaykovich, Phys. Rev. Lett. **108**, 210406 (2012).
[11] C. Chin and P. S. Julienne, Phys. Rev. A **71**, 012713 (2005).
[12] J. F. Bertelsen and K. Molmer, Phys. Rev. A **73**, 013811 (2006).
[13] Th. M. Hanna, Th. Kohler, and K. Burnett, Phys. Rev. A **75**, 013606 (2007).
[14] C. Klempt, T. Henninger, O. Topic, M. Scherer, L. Kattner, E. Tiemann, W. Ertmer, and J. J. Arlt, Phys. Rev. A **78**, 061602(R) (2008).
[15] E. Liverts, B. Bazak, and N. Barnea, Phys. Rev. Lett. **108**, 112501 (2012); B. Bazak, E. Liverts, and N. Barnea, Few-Body Syst. (to be published).
[16] We adopt the Heaviside-Lorentz units in this paper.
[17] L. D. Landau and E. M. Lifshitz, *Quantum Mechanics*, 3rd ed. (Pergamon, New York, 1991).
[18] B. R. Levy and J. B. Keller, J. Math. Phys. **4**, 54 (1963).
[19] L. D. Landau and E. M. Lifshitz, *Statistical Physics*, 3rd ed. (Pergamon, New York, 1980).